Origins of the Cottonwood Canyon fault rock in the Catalina Schist

Justine G. Grabiec

Advisers: Sarah Penniston-Dorland, Richard Walker, & Melodie French

GEOL393: Proposal

Fall 2016

0. Abstract

Interpreting local structures and their role in a large scale system is important for understanding subduction zone and metamorphic processes. In the Catalina Schist of Santa Catalina Island, California, mélange associated with subduction processes consists of large blocks in a fine-grained matrix. This mélange is thought to have formed from the mixing of mafic and ultramafic protoliths, though the mixing processes themselves are poorly understood. The mélange shares a boundary with a coherent amphibolite unit. Within the coherent amphibolite and near this boundary is the Cottonwood Canyon fault with displacement on the centimeter scale and with thicknesses ranging from 15-150 cm over a distance of only about 10 m. Standard models comparing fault thickness and fault displacement cannot explain the thickness characteristics of this fault as the thickness of the fault core is uncharacteristically large for a low-displacement fault. This brings into question the origin of the fault rock. The fault rock may have been derived from the nearby incoherent mélange matrix, the coherent amphibolite hosting the fault, or a combination of both. The Cottonwood Canyon fault may demonstrate the dynamics of the mélange matrix, an incoherent portion of the mélange. The origin of the fault rock may also have implications for the timing of the formation of the fault relative to subduction; the mélange matrix would have been more likely to flow into a system during a warm period characteristic of subduction than during a cool period characteristic of exhumation. A variety of geochemical and petrographic techniques are implemented to test the hypothesis that the fault rock was in part derived from the mélange matrix. X-ray fluorescence is used to determine the major and trace element concentrations and thermal ionization mass spectrometry is used to determine Os concentrations and $^{187}Os/^{188}Os$ ratios. Inductively coupled plasma mass spectrometry is used to determine other highly siderophile elements (HSE) concentrations, including those of Re, Ru, Pt, Ir, and Pd. Electron probe microanalysis (EPMA) and petrography are used to determine the mineralogy of samples, and petrography is also used to identify deformation microstructures in the form of fractures, folds, kinked grains, and evidence of crystal lattice strain. Magnesium, Cr, and Ni concentrations are expected to be high in more ultramafic rocks because the mantle is enriched in Mg and because Cr and Ni are both compatible elements. Amphibolite far from the fault has the expected relatively low concentrations of these elements. So far, the results show that amphibolite close to the fault and the fault rock itself have variable, but relatively higher, Cr and Ni concentrations compared to the host amphibolite far from the fault, as well as variable Mg concentrations. Preliminary mineralogical observations using petrography indicate that the dominant amphibole in the fault rock is a colorless amphibole, while the amphibole in the host amphibolite is hornblende. These differences in mineralogy in transect one, once confirmed with EPMA, may be used to constrain the temperature of the system during fault formation. Deformation microstructures reveal different types of deformation during fault formation including fractures, microfolds, and other evidence of strain. Highly siderophile element (HSE) concentrations, and calculated initial $^{187}Os/^{188}Os$ datum for one host amphibolite sample are consistent with basaltic protolith. Further analysis of Os isotopes and HSEs in fault and host rock samples will be conducted. Extensive petrographic analysis of transects two and three will be conducted to more fully characterize deformation microstructures and at least one more EPMA session will be conducted to confirm mineral identification.

1. Introduction

The Catalina Schist is a metamorphic rock complex on Santa Catalina Island off of the coast of southern California, approximately 40 miles south of Los Angeles. The complex contains subduction-related metamorphic rocks that record the mechanisms and processes taking place during subduction and exhumation. In this study, I investigate the deformation and metamorphism of amphibolite facies mélange and a coherent amphibolite unit, which are included in the Catalina Schist (Fig. 1). Part of the amphibolite facies mélange is the mélange matrix that formed from mafic and ultramafic protoliths.

DRUM note:

Image has been removed from this paper due to copyright restrictions.

Fig. 1. The mélange dominated amphibolite facies rocks and dominantly coherent amphibolite facies (host rock) are the focus of this research. The red box indicates the location of the Cottonwood Canyon fault (adapted from Platt, 1975).

Fault core thickness is thought to scale with the amount of displacement on a fault, but the relationship depends on lithology and other factors such as rock porosity; Shipton et al. (2006) studied this relationship in multiple lithologies. Amphibolite was not one of the lithologies studied, however the closest lithology to amphibolite studied and the one that the amphibolite fault characteristics will be compared to is granite. Expected fault core thicknesses of low-displacement faults in granite, and thus in the Cottonwood Canyon fault, are an order of magnitude larger than what is observed in the Cottonwood Canyon fault (Shipton et al., 2006). Furthermore, upon initial observation, the rock within the fault appears mineralogically different from the amphibolite host rock. This discrepancy brings into question the origin of the fault rock as well as the timing and nature of the formation of the fault. The hypothesis to be tested is that the fault rock was in part derived from the nearby mélange matrix. The null hypothesis is the fault rock was derived from the local amphibolite host rock. It is also possible that the fault rock was derived from both the mélange matrix and the host amphibolite.

The proposed hypotheses will be tested in a variety of ways. The relative abundances of Mg, Ni, Cr, and highly siderophile elements (HSEs) as well as the $^{187}Os/^{188}Os$ ratio of the fault rock will be compared to those of the host amphibolite. Mg, Ni, Cr, and Os are all enriched in the mélange matrix relative to amphibolite blocks in the mélange (Penniston-Dorland et al., 2012). Similar Mg concentrations in the host amphibolite and fault rock would imply that the fault rock was derived from the host amphibolite whereas higher Mg concentrations in the fault rock compared to the host amphibolite would imply that the fault rock was in part derived from the mélange matrix. Thus, similar concentrations of these elements in both the host amphibolite as

well as the fault rock will imply the fault rock is derived from the host amphibolite. On the other hand, if the Ni and Cr concentrations are higher in the fault rock than the host amphibolite, the fault rock was likely in part derived from the mélange matrix. While Os is a compatible element, Re is an incompatible element, so Re is enriched in mafic rocks and depleted in ultramafic rocks. Thus, radioactive decay of the radioisotope ^{187}Re to ^{187}Os would result in a higher $^{187}Os/^{188}Os$ ratio in mafic rocks compared to ultramafic rocks. If the $^{187}Os/^{188}Os$ ratio in the host amphibolite is similar to that of the fault rock, the fault rock was likely derived from the host amphibolite. However, if the $^{187}Os/^{188}Os$ ratio in the fault rock is lower than that of the host amphibolite, then the fault rock was likely derived in part from the mélange matrix. Finally, HSE patterns of the rinds on blocks that formed the mélange matrix are similar to those of peridotites (Penniston-Dorland et al., 2012). Fault rock HSE patterns similar to peridotites would imply mélange matrix origins whereas fault rock HSE patterns similar to those determined of the host amphibolite would imply host amphibolite origins.

Mineral assemblages and deformation microstructures of the fault rock and the host amphibolite will be identified and compared. Differences in mineral assemblages between the host amphibolite and fault rock would imply that the fault rock was derived from a source different than the amphibolite host rock. Furthermore, mineralogical similarities between the fault rock and the mélange matrix would further indicate that the fault rock was derived from the mélange matrix. Specific minerals within the fault rock samples may also hold implications for temperatures of the system during fault formation.

2. Geologic Background

2.1 The Catalina Schist

The Catalina Schist consists of various amphibolite, blueschist, and lawsonite-albite facies rock units (Fig. 1). The coherent amphibolite and mélange-dominated amphibolite facies units are the focus of this study. The mélange contains mafic and ultramafic blocks in a fine-grained matrix containing talc, chlorite, amphiboles (anthophyllite and calcic-amphibole), and enstatite. Zircon, rutile, apatite, spinel, and Fe-Ni sulfides occur as minor phases (Bebout & Barton, 2002). The coherent amphibolite is a coarse-grained rock predominantly containing lineations of hornblende, and, to a lesser extent, plagioclase and epidote. Rutile and oxides are also variably present as minor phases in the coherent amphibolite. The Catalina Schist as a whole reached temperatures up to 350-740°C and pressures up to 7.5-11.5 GPa (Bebout, 2007).

2.2 The Mélange Matrix

It is hypothesized that the mélange matrix formed through tectonic mixing processes and metasomatic alteration of mafic and ultramafic blocks (Bebout & Barton, 2002), as illustrated in Fig. 2. Evidence suggesting fluid infiltration of the system was documented by Sorensen and Barton (1987), Bebout and Barton (1989), and others. As aqueous fluids infiltrated the system, metasomatism altered the outer edges of the blocks. As indicated by petrological and geochemical analysis performed by Sorensen (1988) and Sorensen and Grossman (1989), the altered rims, or "rinds," formed as blocks exchanged components separately with both peridotites and the rinds. More specifically, the blocks gained components from peridotites and lost components to the rinds. Ca- and Mg-rich and Na- and Al- poor clinopyroxenes imply this exchange, as do geochemical

data of garnets and amphiboles obtained via electron probe microanalysis (EPMA). The garnets in rocks containing rinds are enriched in Mg and Fe and are depleted in Ca relative to garnets in rocks without rinds. Some rinds and mélange matrix also contain abundant amounts of anthophyllite, talc, and quartz; such an assemblage is representative of a system reaching about 750˚C (Sorensen and Barton, 1987). As these rinds flaked off, they contributed to the mélange matrix and the process continued during subduction in a relatively warm environment (Sorensen, 1988). The flakes accumulated, ultimately forming the relatively incoherent mélange matrix unit that is in between mafic and ultramafic in composition (Bebout and Barton, 2002). Sorensen (1988) also found that some of the mafic blocks experienced some degree of migmitization.

DRUM note:

Image has been removed from this paper due to copyright restrictions.

Fig. 2. Formation of the mélange matrix as mafic and ultramafic blocks are tectonically and metasomatically altered (Bebout & Penniston-Dorland, 2016).

4. Fault

The Cottonwood Canyon fault is a steeply dipping fault. The fault is variable in thickness and the fault rock is variable in mineralogy. Towards the thinner portion of the fault, the fault has a width of about 15 cm and tapers to an end. Across the middle of the exposed fault and further away from the thinner portion, the fault thickens to about 1.5 m along a distance of about 10 m. Offsets in the host rock near the thin portion of the fault indicate fault displacement of less than 10 cm. Although not part of the study, a steeply dipping conjugate fault is apparent near the thin portion of the main fault and a potential splay of the fault is located in the thicker portion of the main fault (Fig. 3). Fault rock in the thin portion is somewhat incoherent and distinctly green in color. The rock within the fault in the middle of the exposed fault is more incised than the host amphibolite and distinctly different in color than the fault rock in the thin portion as it is less green and more grey.

4. Samples

Eighteen samples were collected throughout three transects along the fault – one across the thin portion, a second across the middle of the exposed fault, and a third across the widest portion of the fault – from which 16 samples were made into thin sections. In total, five samples collected are of the host amphibolite; four were within a meter of the fault while a fifth was collected 64 meters away. The other 13 samples collected are fault rock.

5. Analytical Methods

Billets for all samples except A16-01A and -11 were cut and sent to Spectrum Petrographic Incorporated to make thin sections 30 μm thick. Twelve samples – three host amphibolite and nine

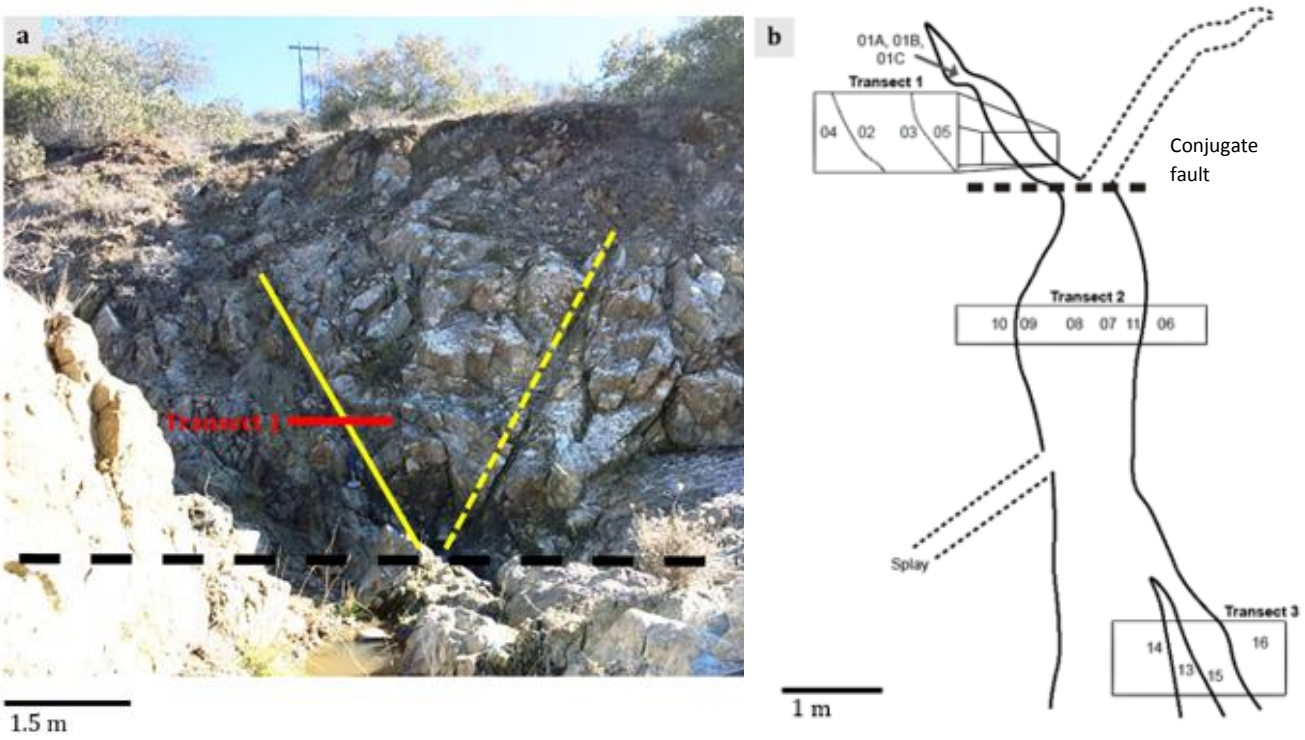

Fig. 3. a) The vertical wall contains the thin portion of the fault core and part of the middle of the exposed fault that contains the thicker portion of the fault core. The solid yellow line marks the beginning of the studied fault. The dashed yellow line marks a possible conjugate fault that will not be a focus of the study but is still an interesting feature nevertheless. b) This outline of the fault as a whole displays the three transects as well as the possible conjugate fault and a potential splay of the fault. The numbers represent the location of sample collection, all of which are labeled with the prefix "A16-" followed by the number and letter combination found above. Sample A16-12 is not pictured, as it was collected 64m away from the fault. The horizontal, bold, black dashed line is located on the same area of the fault in each image.

fault rock - were crushed into fine powders for X-ray diffraction (XRF), thermal ionization mass spectrometry (TIMS), and inductively coupled plasma mass spectrometry (ICP-MS) data collection.

5.1 Petrography

Thin sections were examined to determine mineralogy and note deformation microstructures. The microscope used was a Nikon Eclipse LV1000POL and minerals were identified based on their optical properties in transmitted light. A comparison of the mineralogy of the fault rock to that of the host amphibolite may provide important implications for the relative timing and temperatures of the fault formation and the type of environment in which the fault formed.

Deformation microstructures also provide some insight into the dynamics of and conditions present during fault formation. For example, microfractures and grains present in the fault rock are evidence of mechanical mixing. Altered rims of grains in the fault rock indicate that the fault rock was locally derived and subjected to both chemical and mechanical mixing.

5.2 XRF

The samples analyzed by XRF were sent to Franklin & Marshall College which used a PANalytical 2404 X-ray fluorescence vacuum spectrometer, a PW2540 X-Y sample handler, and 4KW Rh super sharp X-ray tube. Relative standard deviation (RSD) for major elements is <0.6%. For trace elements with concentrations above 25 ppm, the RSD is <5%, except for Cr, which is 12.7%. Trace elements with concentrations lower than 25 ppm have RSDs less than 35%. Loss on ignition (LOI) was first determined by heating a specific amount of a sample for an hour at 950°C. Major element concentrations are determined by creating a glass disk with a flat surface from molten sample. X-rays then interact with a flat side of this disk; it is from these interactions that the major element concentrations are determined. Trace element concentrations are determined from sample briquettes formed by applying a considerable amount of pressure (50,000 psi) to the powdered samples. The methods followed and standards used are those outlined by Penniston-Dorland et al. (2014).

5.3 EPMA

EPMA is used to further identify minerals in order to define the mineralogy of the fault rock and host amphibolite. The instrument used is a JXA-8900 SuperProbe which is a high resolution scanning electron microscope and wavelength-dispersive/energy-dispersive combined electron probe microanalyzer. Data collected during the session are energy-dispersive X-ray spectroscopy (EDS) spectra. The probe current used during the EDS analysis was 0.02506 µA and the beam had a voltage of 15.0 keV. The beam size ranged between 1 and 100 µm, and was adjusted accordingly to avoid any mineral inclusions.

5.4 HSE Geochemistry

HSE concentrations hold implications for the protoliths of the host amphibolite and fault rock. Os is oxidized to its highest valence state of +8 with enriched isotopes of Os and the other specific HSEs in question to make Os easily separable from the rest of the sample. The spikes added to the samples are enriched with ^{185}Re, ^{190}Os, ^{191}Ir, ^{99}Ru, ^{195}Pt, and ^{105}Pd. Furthermore, HSEs, including Os, Re, Ru, Pt, Ir, and Pd, are concentrated in trace alloys and sulfides. Thus, in order to measure the concentration of the HSEs, these phases must be dissolved with aqua regia, a mixture of HCl and HNO_3, and placed in an oven in sealed Carius tubes. A blank is also analyzed to determine how much Os and other HSEs are contributed to the sample from non-sample sources. The HSE separation methods closely follow those of Becker et al. (2001) and Becker et al. (2006). Osmium is chemically separated from the rest of the HSEs, at which point the rest of the HSEs are further separated via column chemistry and chromatography. A more detailed overview of the geochemical separation methods can be found in Appendix I. The concentration of Os and the ^{187}Os/^{188}Os ratio are determined using a Thermo Fisher Triton TIMS. Various HSE isotope ratios for isotope dilution are determined using a Nu Plasma multi-collector ICP-MS from which the HSE concentrations are calculated.

6. Results

Powdered samples have been sent to Franklin and Marshall College for XRF analysis, from which the data were obtained. One amphibolite sample has been geochemically broken down and analyzed for HSEs and the ^{187}Os/^{188}Os ratio. An initial session of EPMA has been conducted to

confirm mineral identities in some of the samples. Thorough analysis of transect one thin sections to determine mineralogy and to identify deformation microstructures has been completed.

6.1 Mineral Assemblages

The host amphibolite is a relatively homogenous rock in terms of mineralogy. The most abundant mineral is hornblende (a clinoamphibole) with a lineation defined by a preferred orientation. Other minerals include variable amounts of plagioclase and epidote, both of which are also defined by a lineation, and quartz. Rutile and an iron oxide are present as minor phases. The fault rock, on the other hand, is heterogeneous not only between transects but also between different samples collected in the same transect. In transect one, for example, there is a colorless amphibole present that is different from the hornblende clasts seemingly derived from the host amphibolite (Fig. 4). The composition of this colorless amphibole will be determined with wavelength-dispersive X-ray spectroscopy (WDS) during a second EPMA session.

The amphibole present in the host amphibolite is predominantly hornblende, some of which seems to be present as clasts that broke off of the host amphibolite into the fault rock. Therefore, these hornblende clasts in the fault rock are inconclusive for relative temperatures of fault formation as they were likely emplaced, not crystallized, during fault formation. On the other hand, the dominant, colorless amphibole in the fault rock may be anthophyllite and may have constraining implications. The presence of anthophyllite in the fault rock would imply that the fault formed under higher temperature conditions of 660-760°C as reported by Sorensen and Barton (1987) and Greenwood (1963). Anthophyllite is present as a major phase in the mélange matrix and may be the identity of the dominant amphibole in the fault rock. Thus, the temperature range of crystallization of anthophyllite may imply that the fault rock formed during a warm, subducting system.

In terms of trace elements, EDS via EPMA confirmed the presence of rutile and red iron oxides in some, but not all, of the host amphibolite samples. Some fault rock close to the host amphibolite in transect two also contained allanite grains, as characteristic Th peaks and the presence of other REEs were apparent in the EDS spectra (Fig. 5.). Allanite is commonly found in

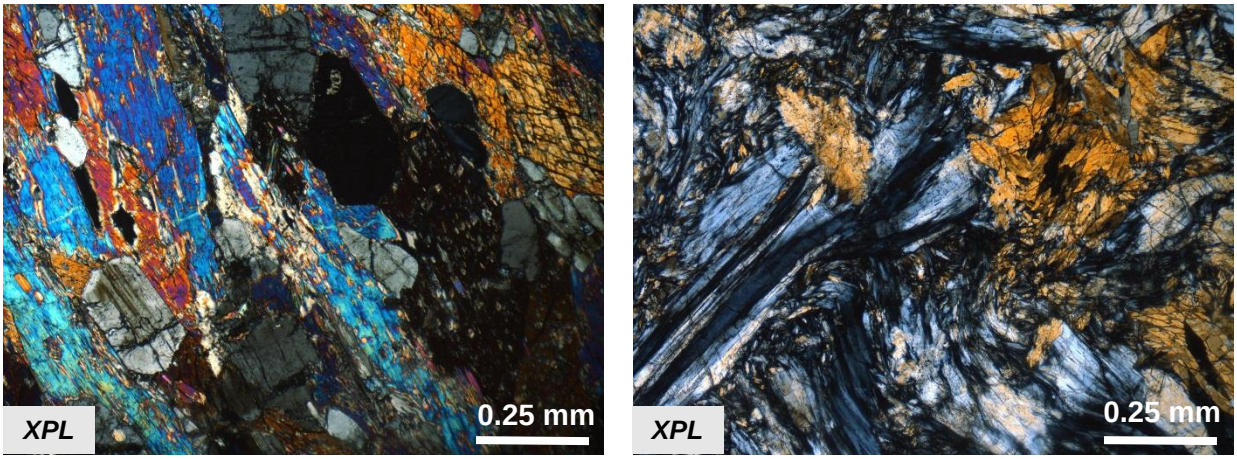

Fig. 4. Left image: Sample A16-04 is from the left side of the host rock in transect one. The oriented amphiboles with relatively high birefringence are hornblendes and the euhedral grains are epidote. Right image: Sample A16-01C is from the upper portion of the fault rock from the thin portion of the fault core. The lower birefringent mineral is a colorless amphibole, but whether or not it is an orthoamphibole (such asanthophyllite) is still unclear.

amphibolite (Gieré and Sorensen, 2004). Finally, the portion of the fault rock from which sample A16-13 was collected was less incised than the rest of the fault rock and contains a soft, white, fibrous mineral not yet identified.

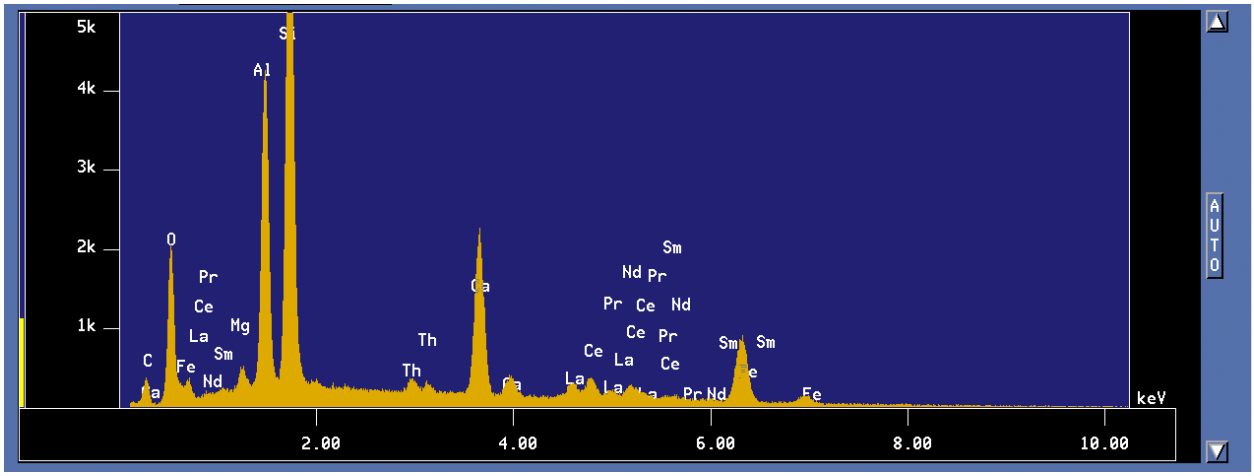

Fig. 5. The characteristic EDS spectrum of allanite with the Th peak and other REE peaks labeled. Allanite is an epidote mineral generally found with a high concentration of REEs (Gieré and Sorensen, 2004).

6.1.1 Mineralogy of Transect 1

The mineralogy of the first transect along the thin portion of the fault is summarized in Fig. 6. More complete mineral descriptions of each sample can be found in Appendix II. The main mineral present in many of the fault rock samples is a colorless amphibole, but the type of amphibole is currently unknown so more analysis needs to be conducted. The amphiboles and other mineral identities not already confirmed, including an unknown yellow mineral found in the fault rock, will be subjected to WDS via EPMA.

6.2 XRF

The XRF data for the twelve powdered samples are summarized in Table 1. As compatible elements, Ni and Cr are expected to be relatively higher in concentration in ultramafic rocks than in mafic rocks. Thus by comparing XRF data for these two elements in the fault rock and the host amphibolite, it may be possible to constrain the origin of the fault rock. The compositions of the samples will also be compared to that of the mélange matrix, which has enrichments of Mg, Ni, and Cr relative to amphibolite. Out of the three host amphibolite samples analyzed with XRF, two were collected from the boundary of the fault and have concentrations of Ni and Cr similar to those of the fault rock. On the other hand, the third host amphibolite sample, A16-12, was collected 64 meters away from the fault and has relatively lower concentrations of these elements, which is what is expected of a typical amphibolite. Thus, the discrepancy of Ni and Cr concentrations in the host amphibolite raises questions about the origin of the unexpectedly high amounts of Ni and Cr in the host amphibolite close to the fault. As noted by Chester et al. (1993), rock immediately surrounding fault cores tends to be fractured and is commonly infiltrated by fluid, which may be a source of the excess Ni and Cr in the host amphibolite close to the fault.

6.2.1 Mg, Ni, and Cr in Transect 1 Samples

Sample A16-01B was collected where the fault is thinnest in the studied outcrop (about 15 cm). For comparison, the fault is a few centimeters thicker where samples A16-02 or A16-03B were collected (about 20 cm). Samples A16-02 and A16-03B have Mg concentrations that are an order of magnitude higher than those of sample A16-01B, which initially seem to imply that the fault rock closer to the thinner portion has a more mafic protolith while the lower two samples may have a relatively more ultramafic protolith. This may also be accounted for by the different amphiboles present in the samples. Fig. 7 presents the Cr, Ni, and MgO concentrations as contour maps, which indicate that the concentrations of these elements generally increase towards the center of the fault. The sample of host amphibolite collected 64 m away from the fault (sample A16-12) also has lower concentrations of these elements than the host amphibolite samples collected close to the fault boundary.

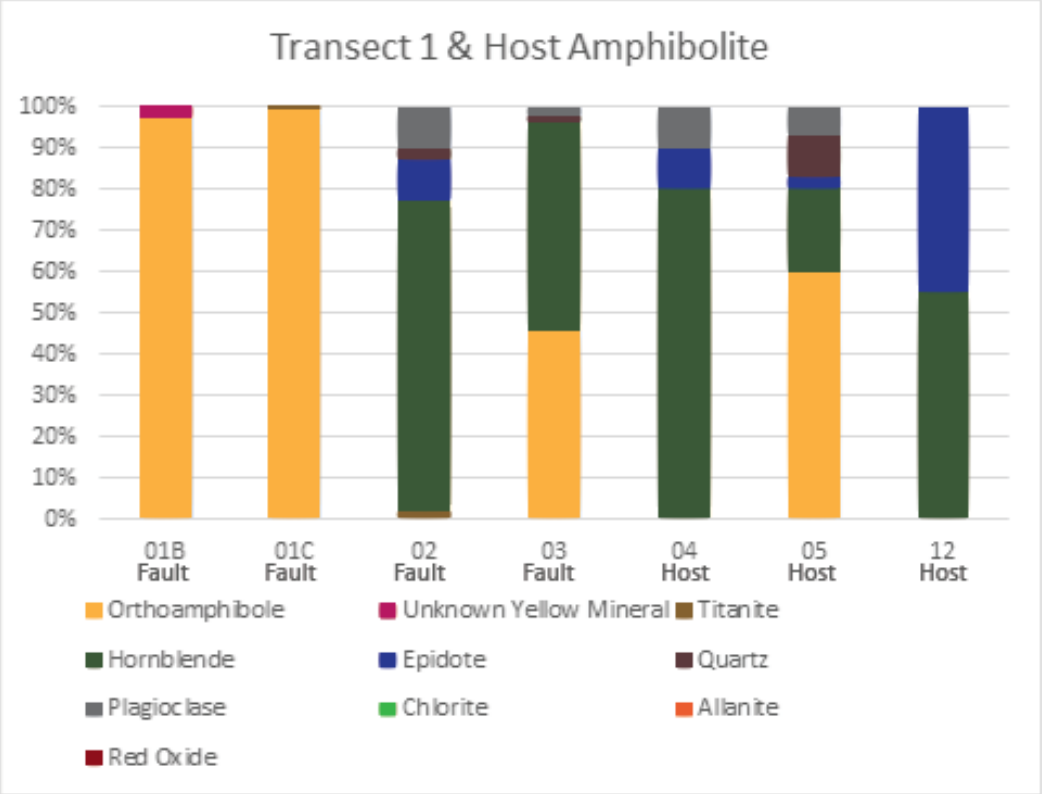

Fig. 6. The modal mineralogy of transect 1 as compared to the host rock sample 64m away from the fault. Sample A16-12 is host amphibolite 64 m away from the fault whereas samples A16-04 and -05 are host amphibolite samples along the boundary of the fault.

6.3 Osmium Concentrations & $^{187}Os/^{188}Os$ Ratios

One sample (A16-12, the host amphibolite 64 m away from the fault) has been analyzed for HSEs. The data can be found in Table 2. This host rock appears to have the similar HSE concentrations of mafic blocks in the mélange matrix, some of which are garnet amphibolite. Primitive upper mantle-normalized HSE concentrations, plotted of basalts and peridotites in Fig. 8, and a calculated initial $^{187}Os/^{188}Os$ ratio of 0.390 (γ_{Os}= +238), are also consistent with sample A16-12 having had a mafic protolith (Penniston-Dorland et al., 2012).

Specimen	T1 Fault A16-01B	T1 Fault A16-02	T1 Fault A16-03B	T2 Host A16-06	T2 Fault A16-07	T2 Fault A16-08	T2 Fault A16-09	T2 Host A16-10	T3 Host A16-12	T3 Fault A16-13	T3 Fault A16-14	T3 Fault A16-15
SiO_2	40.61	42.25	46.68	50.33	54.70	51.84	51.93	42.56	45.03	50.37	53.66	46.86
TiO_2	0.05	1.16	0.66	0.27	0.00	0.09	0.45	1.45	0.32	0.09	0.04	0.16
Al_2O_3	27.46	15.70	13.10	9.55	2.19	4.48	15.47	14.54	18.32	5.24	3.33	17.98
Fe_2O_3	3.08	14.74	9.93	8.51	8.42	9.93	9.44	15.30	7.15	11.95	9.81	5.29
MnO	0.19	0.19	0.15	0.16	0.25	0.15	0.17	0.22	0.13	0.17	0.14	0.10
MgO	4.13	13.58	14.24	16.84	22.36	23.13	10.96	15.09	11.06	23.06	21.73	10.75
CaO	23.88	10.90	13.93	11.98	11.43	9.98	6.68	9.25	15.95	8.60	11.00	17.04
Na_2O	0.25	0.88	0.94	1.81	0.33	0.27	4.33	1.22	1.64	0.25	0.24	1.07
K_2O	0.000	0.051	0.098	0.267	0.024	0.016	0.382	0.121	0.153	0.012	0.019	0.295
P_2O_5	0.003	0.218	0.024	0.004	0.007	0.001	0.008	0.007	0.011	0.003	0.002	0.007
Total	**99.653**	**99.669**	**99.752**	**99.721**	**99.711**	**99.887**	**99.820**	**99.758**	**99.764**	**99.745**	**99.971**	**99.552**
LOI	7.11	4.78	4.99	1.46	2.80	4.42	2.76	4.86	0.78	6.14	3.66	1.06
Rb	1.2	<0.5	0.5	3.5	<0.5	<0.5	8.8	1.7	1.8	<0.5	<0.5	6.4
Sr	5	197	14	26	10	9	130	26	274	7	6	235
Y	4.4	75.7	24.8	9.0	9.7	5.9	61.3	74.5	15.4	3.1	3.8	13.9
Zr	11	273	26	14	10	10	141	139	22	11	10	14
V	181	357	157	160	33	75	185	301	174	63	49	124
Ni	102	332	352	487	630	672	202	388	209	1057	763	207
Cr	128	574	737	1460	1675	2435	526	1165	478	2376	1053	651
Nb	<0.5	10.1	0.7	<0.5	<0.5	<0.5	1.0	11.4	<0.5	<0.5	<0.5	<0.5
Ga	15.0	16.1	10.2	8.0	3.5	7.5	11.1	12.5	12.9	7.6	5.6	14.0
Cu	31	209	180	40	624	168	146	201	63	123	101	51
Zn	28	118	64	49	64	63	85	147	48	67	62	37
Co	4	56	57	59	51	64	31	64	42	100	50	31
Ba	20	15	22	165	<3	16	393	61	82	9	5	136
La	12	17	8	9	8	6	22	9	8	8	6	10
Ce	9	46	11	9	6	5	55	17	13	3	10	12
U	<0.5	1.5	<0.5	<0.5	<0.5	<0.5	<0.5	<0.5	0.5	<0.5	<0.5	<0.5
Th	<0.5	15.4	<0.5	<0.5	<0.5	<0.5	13.2	4.0	<0.5	1.0	<0.5	<0.5
Sc	21	38	53	44	10	15	27	33	43	12	16	46
Pb	10	<1	3	<1	<1	<1	<1	<1	<1	<1	<1	1

Table 1. XRF data collected at Franklin & Marshall College. T1, T2, and T3 refer to transects 1, 2, and 3 respectively, as illustrated in Fig. 2. Samples are positioned in order of collection along the traverse. Major elements are reported as oxides in weight percent and trace elements are reported in parts per million.

6.4 Deformation Microstructures

A significant portion of the deformation microstructures identified with petrography have been microfolds, kinked grains, and fractures. Microfolds represent distributed rather than localized deformation and are apparent throughout the transects. Kinks occur in various minerals including hornblende and epidote grains (Fig. 9). Fractures are present across thin sections and multiple grains, but are less frequent in individual mineral grains. Some fractures seem to have altered texture of mineral grains crosscut by the fractures.

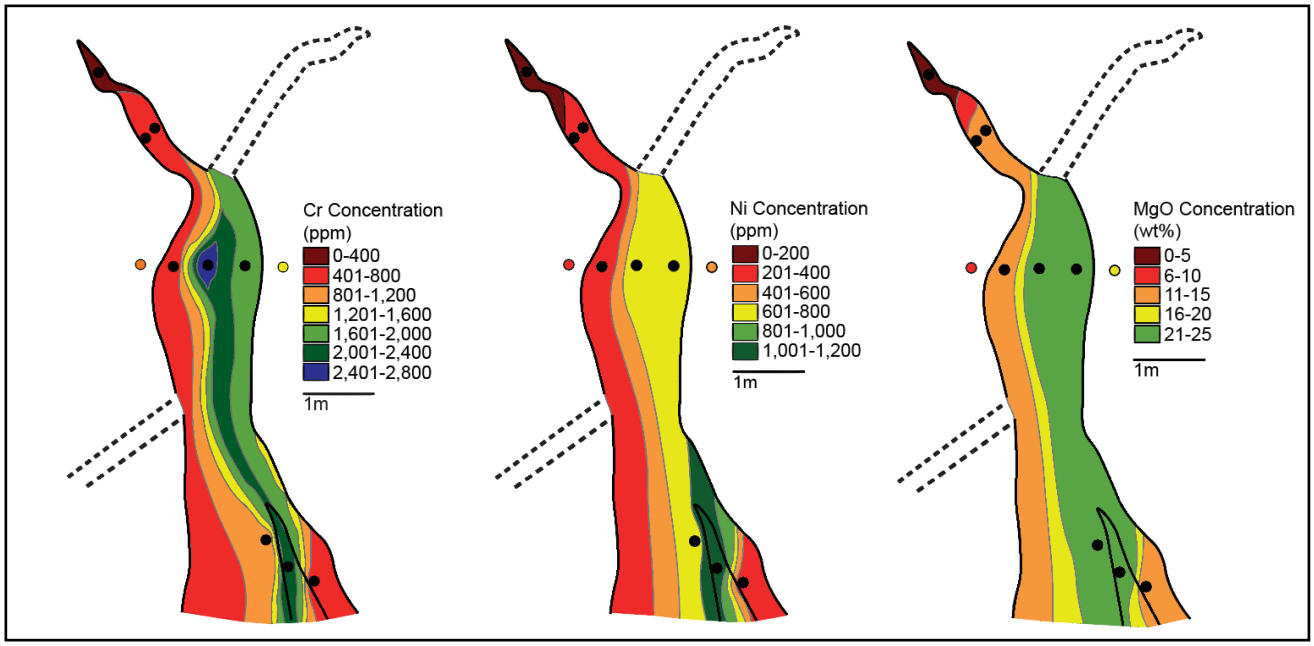

Fig. 7. Contour maps showing absolute concentrations of Cr, Ni, and MgO in the fault material indicate higher concentrations towards the center right portions of the fault rock. Black circles indicate samples of fault rock. Colored circles indicate samples of host rock. For comparison, the sample A16-12 (host amphibolite collected 64 m away from the fault) has Cr, Ni, and MgO concentrations of 478 ppm, 209ppm, and 11.06 wt%, respectively.

a)	Os	Ir	Ru	Pt	Pd	Re
Concentration (ppb)	0.0068	0.00093	0.0043	0.16	0.28	0.0058
Uncertainty (%)	0.12	12	44	52	3.0	6.2

b)	$^{187}Os/^{188}Os$	$^{187}Re/^{188}Os$	$^{187}Os/^{188}Os_{initial}$
Uncertainty (%)	0.382	4.20	0.374
	0.273	6.26	0.160

Table 2. The concentrations of the analyzed HSEs and their uncertainties are presented above. The Os concentration and isotope ratio are similar to those of the mafic amphibolite blocks reported in Penniston-Dorland et al. (2012). a) Ir, Ru, Pt, Pd, and Re uncertainties are reported as percentages of blanks contained within the sample prior to blank correction. The Os concentration is reported as two standard error. b) $^{187}Os/^{188}Os$ ratio uncertainty is reported as two standard error. $^{187}Re/^{188}Os$ ratio uncertainty is reported as percentages of blanks contained within the Re sample prior to blank correction and $^{187}Os/^{188}Os_{initial}$ ratio uncertainty is reported as the change in ratio if uncertainty from the $^{187}Re/^{188}Os$ ratio is considered. The age used to calculate $^{187}Os/^{188}Os_{initial}$ is 114.5 Ma, which was used by Penniston-Dorland et al. (2012) to calculate $^{187}Os/^{188}Os_{initial}$ of mafic blocks. This age was determined by Anczkiewicz et al. (2004).

6.4.1 Deformation Microstructures in Transect 1

Significant folding is present in the fault rock in transect one, implying distributed strain rather than localized strain. Thin section-wide, or transgranular, fractures are observed in the fault rock. A predominantly plagioclase vein is also seen cross-cutting the hornblende lineations in one host amphibolite sample. There are also fractures that seem to drag parts of crystals through which they pass instead of producing a clean offset (Fig. 10).

DRUM note:
Image has been removed from this paper due to copyright restrictions.

Fig. 8. HSE concentrations normalized to the primitive upper mantle (PUM) discriminate between ultramafic and mafic rocks. Triangles represent data from Penniston-Dorland et al. (2012); black triangles are rind samples, white triangles are core samples, and grey triangles are mélange samples. The crosshatched zone is the area where basalts plot; the solid grey zone is the area where peridotites plot. The red squares are the HSE data collected from sample A16-12. As a mafic rock, sample A16-12 is already depleted in HSEs, though this sample in particular is especially depleted in Os, Ir, Ru, and Re compared to the mafic blocks analyzed by Penniston-Dorland et al. (2012).

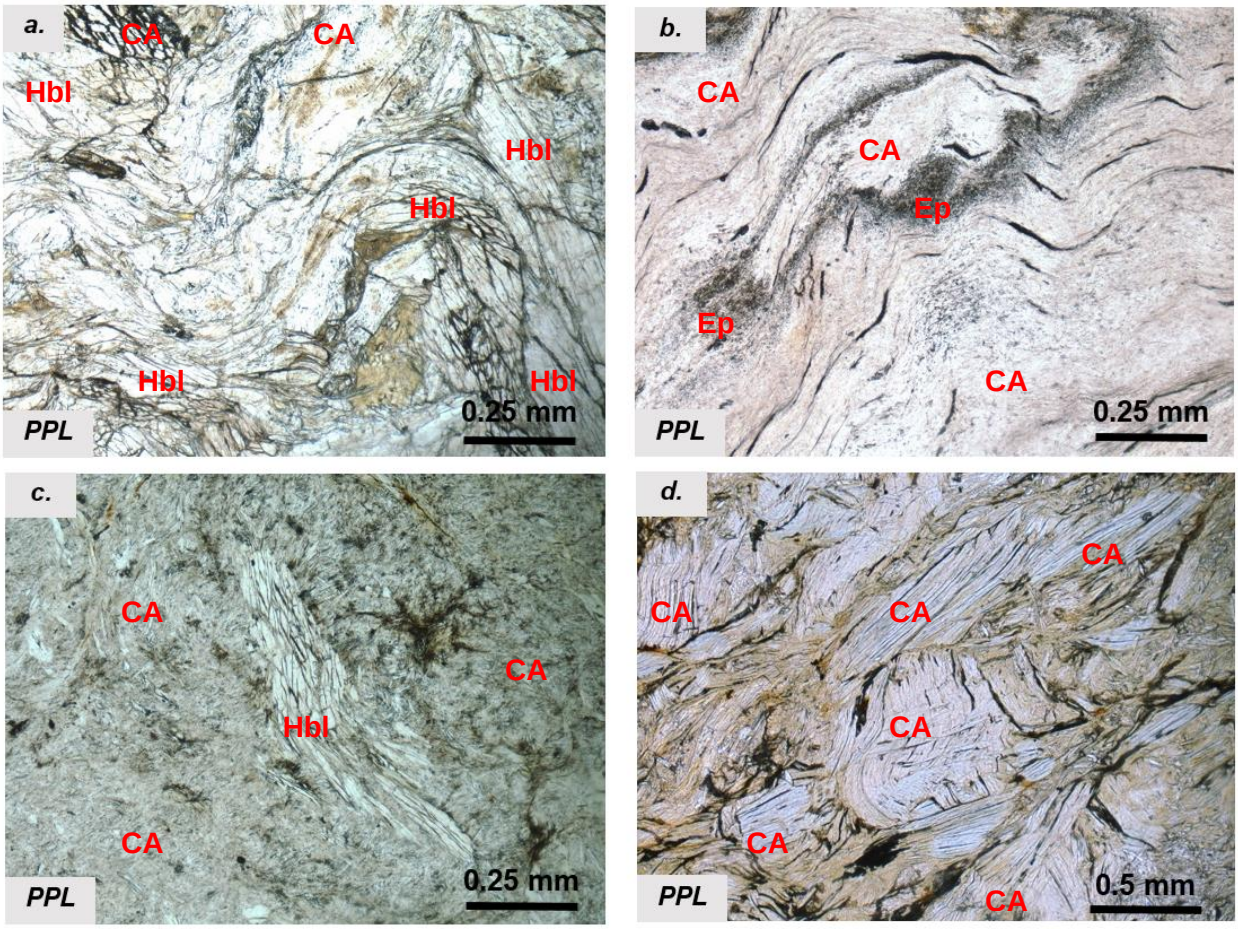

Fig. 9. CA stands for colorless amphibole. a.) Sinusoidal fold in sample A16-03 (fault rock) collected across transect one. The amphibole affected by the strain is hornblende; epidote is also present as the greenish mineral. b.) Small-scale folding in sample A16-08a (fine-grained fault rock) collected along transect two. c.) Partially kinked hornblende grain in sample A16-14 (fine-grained fault rock) collected along transect two. d.) Kinked crystal in sample A16-13 (fault rock) collected across transect three.

Sample A16-05 (right side of host amphibolite close to the fault in transect 1) contains evidence for deformation in the crystal grains. Quartz grains of varying size in the vein have grain boundary migrations and subgrains, indicating strain of the lattice in response to stress. Subgrain migration textures in quartz were formed in a system either increasing in temperature or decreasing in strain rates, and therefore a decrease in flow stress was present in either scenario (Hirth and Tullis, 1991). Deformed quartz grains in a vein implies deformation after the vein was emplaced. Hornblende grains in multiple thin sections exhibited undulatory extinction, also indicating lattice strain in response to stress.

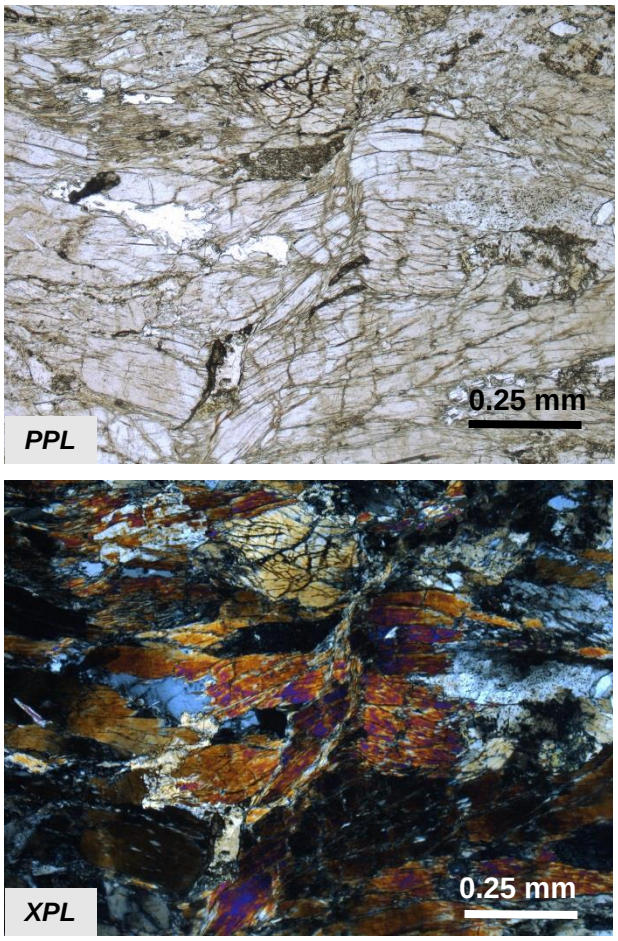

Fig. 10. Sample A16-02 is fault material from the first transect. The hornblende clast is cut through by a fracture. The fracture seems to drag the clast, creating smaller, fine-grained fractures of the clast closest to the fracture, ultimately producing a somewhat deformed, less clean offset.

7. Discussion

As indicated by Fig. 7, there is a general increase of Cr, Ni, and Mg towards the center of the fault rock. Higher Cr and Ni concentrations are expected in ultramafic rocks as these elements are compatible. Ultramafic rocks are also enriched in Mg as they originate in the mantle where Mg is enriched. Thus this general increase of Cr, Ni, and Mg towards the center indicates that the fault rock is more ultramafic in origin than the host amphibolite, ultimately implying that the fault rock was in part derived from the mélange matrix. The host amphibolite from sample A16-12 also has lower Cr, Ni, and MgO concentrations than the host amphibolite collected along the boundary of the fault. Possible enrichments of these elements in the host amphibolite near the fault rock may be due to fluid movement through fractures in the host amphibolite close to the fault caused by fault formation.

The occurrence of two entirely different amphiboles has some important implications. While the host amphibolite is entirely the clinoamphibole hornblende, the amphibole present in the fault rock is almost entirely a colorless amphibole, except for some hornblende clasts likely derived from the nearby host amphibolite. Another EPMA session will reveal whether the colorless amphibole in the fault rock is the orthoamphibole anthophyllite, which will have implications for the temperature of the system during fault formation, as anthophyllite is generally considered a high temperature mineral forming around 660-760˚C (Sorensen and Barton, 1987; Greenwood, 1963). It also may imply that the fault rock was derived from the mélange matrix, where anthophyllite is common (Sorensen and Barton, 1987; Bebout and Barton, 2002). Furthermore, if the colorless amphibole is an orthoamphibole, the fact that there are definitive chemical differences between clinoamphiboles and orthoamphiboles may imply different origins of either amphibole. Orthoamphiboles have a

higher Mg content than clinoamphiboles and clinoamphiboles have a higher Ca content than orthoamphiboles. For example, sample A16-12 is host amphibole from 64 m away from the fault and has 11.06 wt% MgO and 15.95 wt% CaO. On the other hand, sample A16-07 is fault rock from transect two and has 22.36 wt% MgO and 11.43 wt% CaO. This data support the observations that the dominant amphiboles in the host amphibolite and fault rock are the clinoamphibole hornblende and potentially an orthoamphibole, respectively.

Deformation microstructures recognized within the fault rock imply distributed shear during at least part of the history of the fault formation. Furthermore, microfolding within the fault rock as well as individually kinked mineral grains indicate distributed shear. Fractures are also present, though are more frequent as transgranular than intragranular fractures.

8. Future Work

XRF data collection is complete, an initial EPMA session was conducted, and the mineralogy and deformation microstructures of transect one have be described in detail. However, more data needs to be collected and more analysis conducted. At least one more EPMA session will take place to collect EDS and WDS spectra to confirm the mineralogies of the samples. Literature research on the mobility of Ni and Cr in fluids will be conducted. HSE data and $^{187}Os/^{188}Os$ ratios will be collected from at least three more samples (at least one more host rock and at least two fault rock samples). Extensive petrography will be conducted to study the patterns of mineralogies, textures, and deformation microstructures of transects two and three. Furthermore, all results and observations will be compiled, and variations within and among transects will be described and interpreted. Finally, conclusions will be made that support or deny the proposed hypothesis that the fault rock was in part derived from the mélange matrix.

9. Acknowledgments

I would like to thank Drs. Sarah Penniston-Dorland, Melodie French, and Richard Walker for their tireless efforts to train me in the field and lab and to answer my streams of questions. I would also like to thank Dr. Stanley A. Mertzman for collecting the XRF data at Franklin and Marshall College and the Catalina Island Conservancy for their permission to conduct field work. The research was funded by National Science Foundation grant EAR-141987.

10. References

Anczkiewicz, R., Platt, J.P., Thirlwall, M.F., Wakabayashi, J., 2004. Franciscan subduction off to a slow start: evidence from high-precision Lu-Hf garnet ages on high grade-blocks: Earth and Planetary Science Letters, v. 225, p. 147-161.

Bebout, G.E., 2007. Metamorphic chemical geodynamics of subduction zones: Earth and Planetary Science Letters, v. 260, p. 373-393.

Bebout, G.E. and Barton, M.D., 1989. Fluid flow and metasomatism in a subduction zone hydrothermal system: Catalina Schist terrane, California: Geology, v. 17, p. 976-980.

Bebout, G.E. and Barton, M.D., 2002. Tectonic and metasomatic mixing in a high-T, subduction-zone mélange – insights into the geochemical evolution of the slab – mantle interface: Chemical Geology, v. 187, p. 79-106.

Bebout, G.E. and Penniston-Dorland, S.C., 2016. Fluid and mass transfer at subduction interfaces – The field metamorphic record: Lithos, v. 240-243, p. 228-258.

Becker, H. et al., 2001. Rhenium-osmium systematics of calcium-aluminum-rich inclusions in carbonaceous chondrites: Geochimica et Cosmochimica, v. 65, p. 3379-3390.

Becker, H. et al., 2006. Highly siderophile element composition of the Earth's primitive upper mantle: Constraints from new data on peridotite massifs and xenoliths: Geochimica et Cosmochimica Acta, v. 70, p. 4528-4550.

Chester, F.M., Evans, J.P., and Biegel, R.L., 1993. Internal Structure and Weakening Mechanisms of San Andreas Fault: Journal of Geophysical Research, v. 98, p. 771-786.

Gieré, R. and Sorensen, S.S., 2004. Allanite and Other REE-Rich Epidote-Group Minerals: Mineralogical Society of America, v. 56, p. 431-493.

Greenwood, H.J., 1963. The Synthesis and Stability of Anthophyllite: Journal of Petrology, v. 4, p. 317-351.

Hirth, G. and Tullis, J., 1991. Dislocation creep regimes in quartz aggregates: Journal of Structural Geology, v. 14, p. 145-159.

Pennison-Dorland, S.C., Gorman, J.K., Bebout, G.E., Piccoli, P.M., Walker, R.J., 2014. Reaction rind formation in the Catalina Schist: Deciphering a history of mechanical mixing and metasomatic alteration: Chemical Geology, v. 384, p. 47-61.

Penniston-Dorland, S.C., Walker, R.J., Pitcher, L., Sorensen, S.S., 2012. Mantle-crust interactions in a paleosubduction zone: Evidence from highly siderophile element systematics of eclogite and related rocks: Earth and Planetary Science Letters, v. 319-320, p. 295-306.

Platt, J.P., 1975. Metamorphic and deformational processes in the Franciscan Complex, California: Some insights from the Catalina Schist terrane: Geological Society of America Bulletin, v. 86, p. 1337-1347.

Shipton, Z.K., Soden, A.M., Kirkpatrick, J.D., Bright, A.M., and Lunn, R.J., 2006. How Thick is a Fault? Fault Displacement-Thickness Scaling Revisited: American Geophysical Union, v. 170, p. 193-198.

Sorensen, S.S., 1988. Petrology of amphibolite facies mafic and ultramafic rocks from the Catalina Schist, southern California: metasomatism and migmitization in a subduction zone metamorphic setting: Journal of Metamorphic Petrology, v. 6, p. 405-435.

Sorensen, S.S. and Barton, M.D., 1987. Metasomatism and partial melting in a subduction complex: Catalina schist, southern California: Geology, v. 15, p. 115-118.

Sorensen, S.S. and Grossman, J.N., 1989. Enrichment of trace elements in garnet amphibolites from a paleo-subduction zone: Catalina Schist, Southern California. Geochimica et Cosmochimica Acta, v. 53, p. 3155-3178.

Appendix I: Os and HSE Separation Methods

For initial digestion and Os separation, samples are mixed with spikes, put into Pyrex Carius tubes with concentrated HCl, and put into a bucket of ice. Concentrated HNO_3 is added and the Carius tubes are placed in ice again. Once sealed, the Carius tubes are placed in a sealed jacket with a copper gasket and placed into a 220-240°C oven. Each sample requires a 15 mL Teflon container and a 60 mL centrifuge tube that have been cleaned, rinsed, dried, and labeled with the appropriate sample number. Each sample is designated three 5 mL pipette tips, labeled with the word acid, the word solvent, or the respective sample number. Three mL of carbon tetrachloride solution (CCl_4) is added to each centrifuge tube. Four mL of concentrated HBr is added to each Teflon container. The Carius tubes are frozen, opened, and thawed, and contents are poured into the centrifuge tubes which are then placed in the centrifuge for one to three minutes. With the designated sample pipetter tip, CCl_4 is pipetted from the bottom of the centrifuge tube into the Teflon containers containing the HBr. Three mL of CCl_4 is added to the centrifuge tube and centrifuged again. The CCl_4 is removed from the centrifuge tube and placed into the Teflon containers and this step is repeated once more. The pipetter tips are then rinsed and saved for later use. The sealed Teflon containers are placed on an 85°C hotplate for at least two hours but no longer than overnight. Once cooled, the CCl_4 is extracted from the bottom of the Teflon container and placed in a waste bottle. The Teflon container is then placed below a heat lamp where the HBr dries until it is about a 40 µL droplet. Caps and bottoms of 5 mL conical bottom Teflon vials are labeled for each sample. With a clean 50-200 µL pipetter tip, 40 µL of HBr is removed from the 15 mL Teflon container and placed in the flat cap, which is then placed under a heat lamp, and capped once dry.

Once the above process is completed, the now-dry Os sample is ready for micro-distillation. Fifteen µL of concentrated HBr is placed in the tip of a 5 mL conical bottom Teflon vial cap, ensuring that all of the HBr is at the bottom. About 20-30 µL of dichromate solution is added to the flat cap containing the dried Os sample. The cap containing the Os and dichromate is screwed onto the vessel containing the HBr, ensuring that the HBr is not shaken from the top. Remaining inverted, the closed vessel is wrapped in aluminum foil, and put on an 85°C hot plate for two to three hours. Following this, the Teflon container is removed from the hot plate and the aluminum foil is removed. Milli-Q (MQ) H_2O is added to the residue to ensure that the distillation was a success; upon MQ addition to the residue, a resultant yellow color indicates successful distillation, whereas a green color indicates insufficient Cr^{+3} ions are oxidizing Os, and that more dichromate needs to be added and the sample redistilled. Once the cap is placed back on the sample, the container containing to HBr rests for a few hours to ensure all of the Os is reduced. Finally the HBr and Os is placed under a heat lamp to evaporate the HBr, after which the Os left behind is loaded onto a clean filament and analyzed via TIMS.

Left behind from the Os separation is the aqua regia and "sludge" which is centrifuged in a 50 mL centrifuge tube for about 5-10 minutes at maximum speed. The aqua regia is then pipetted into the 15 mL Teflon container used previously for the Os separation, and the sludge is placed in acid waste containers. The centrifuge tubes are then rinsed and saved. Once placed under a heat lamp, aqua regia in the 15 mL Teflon tube is dried until very viscous (almost, but not completely, solid). To remove all HNO_3 and lower the normality of the HCl, 2.5-10 mL of 1 N Teflon distilled HCl is added to the Teflon container and placed on the hot plate. The sample is then placed under the heat lamp to partially dry the sample, and then the step of adding HCl and partially drying is repeated once more. Finally, about 2.5 mL of 1N Teflon distilled HCl is placed into the Teflon

container and back onto the hot plate at around 80-90° to completely dissolve the sample. At this point the sample is prepared for column chemistry and chromatography.

In order to conduct the column chemistry and chromatography, cleaned, rinsed, and labeled Biorad 2 mL disposable columns are placed in a column stand with drip cups below. About 1.7 mL anion resin is pipetted into each column. Once the water from the resin drips out, the column and resin can be cleaned. Five mL of MQ H_2O is pipetted into each column and drained, followed by 10 mL of concentrated quartz distilled (QD) HNO_3, 10 mL of concentrated Teflon distilled (TD) HNO_3, 2 mL of MQ H_2O, 10 mL of QD concentrated HCL, 2 mL of MQ H_2O, 2 mL of 1N TD HCl, and 2 mL of 1N TD HCl. After this process, the samples can be loaded into the columns. Once the samples are loaded into the columns, two 6 mL rounds of 1N TD HCL + HF are pipetted into the columns, followed by two 2 mL rounds of 0.8N TD HNO_3. At this point Re and Ru are collected in a cleaned and labeled 15 mL Teflon container by pipetting 12 mL of 6N TD HNO_3. In another cleaned and labeled 15 mL Teflon container, Pt and Ir are collected by pipetting 13 mL of concentrated TD HNO_3 followed by 2 mL of MQ H_2O. Finally, in a third cleaned and labeled 15 mL Teflon container, 14 mL of concentrated TD HCl is pipetted into the column. Once all samples are collected, they are dried separately and completely under a heat lamp, making sure to avoid sample splattering.

To more thoroughly clean the Re + Ru samples, the dried Re + Ru sample is re-dissolved in 0.5 mL 1N TD HCl on an 80˚C hotplate for at least one hour. A clean and rinsed in MQ H_2O 0.25 mL column is placed in a column stand with clean AGIx8 anion resin within 0.5 cm of reservoir base with drip cups below column. Eluted are 2 mL MQ H_2O, followed by 10 mL concentration TD HNO_3, 1 mL MQ H_2O, and two rounds of 2 mL 1N TD HCL. The re-dissolved Re + Ru sample is loaded into the column, followed by two rounds of 1 mL TD HCL and two rounds of 1 mL 0.8N TD HNO_3. In order to collect the Re + Ru, 7 mL 6N QD HNO_3 is put into the column and collected in a 15 mL Savillex container. Two to three drops of concentrated TD HCl and HNO_3 are added to the beaker containing the Re + Ru sample and dried to remove any organics.

It is at this point that all dried HSE samples are ready to be put into solution for ICP-MS analysis. Fifty μL of concentrated HNO_3 are added to samples in Teflon containers at least an hour prior to ICP-MS analysis except for Pd samples. Pd samples should be put into solution as close to analysis as possible as it may be adsorbed into the plastic of the Teflon container once mixed with the HNO_3. Each sample then gets 950 μL of MQ H_2O, and the dissolved sample is transferred to a clean and labeled 1.5 mL centrifuge tube from which the solution is analyzed via ICP-MS.

Appendix II: Mineral Descriptions

Sample A16-01B

Fault rock, upper portion of the thin portion of the fault, transect 1

Minerals

1. Colorless amphibole (97%): Euhedral, some radial elongate crystals, some prismatic; relatively coarse-grained (0.5-15mm); undulatory extinction in some grains; few areas with epidotization
2. Unknown yellow mineral (3%): Anhedral; interstitial occurrence; moderately coarse grained (1-4mm); amorphous; honey-yellow and pink in PPL; not isotropic; high relief
3. Titanite (<1%): 1-3 mm across; euhedral

Deformation Microstructures

- Transgranular fractures, some crosscutting elongate colorless amphiboles
- Colorless amphibole intragranular fractures perpendicular to length

Sample A16-01C

Fault rock, upper portion of the thin portion of the fault, transect 1

Minerals

1. Colorless amphibole (99%): Euhedral to subhedral; variable grain size from radial and coarse (1-15mm) to fine and wispy (<1mm); crystals seem to be groups together based on grain size; undulatory extinction in some grains
2. Titanite (1%): Euhedral; some grouped together; 1-3mm across
3. Unknown yellow mineral (<1%): Anhedral; occupying fracture

Deformation Microstructures

- Transgranular fractures crosscutting zones of differently sized grains
- Intragrain fractures in elongate colorless amphibole grains perpendicular to length
- Small intragrain faulting of colorless amphibole with an offset of about one mm
- Folding in grains and fabric

Sample A16-02

Fault rock, left side closest to host rock, transect 1

Minerals

1. Hornblende (75%): Subhedral; coarse grained (3-30mm); undulatory extinction seen in some grains

2. Plagioclase (10%): Subhedral; simple and albite twinning in some grains; coarse-grained (2-10mm); epidotization
3. Epidote (10%): Subhedral to anhedral; coarse-grained where subhedral (2-30mm), fine-grained where anhedral (<0.5mm); fine-grained as alteration products
4. Quartz (3%): Anhedral; epidotization of some grains; undulatory extinction
5. Titanite (2%): Euhedral; 0.5-3mm

Deformation Microstructures

- Relatively wavy thin section-wide fracture producing deformed mineral grains
- Transgranular fractures
- Intragrain fractures in epidote and hornblende grains crosscutting length; intragrain fractures in various directions in quartz grains
- Some minerals slightly deformed/folded

Sample A16-03

Fault rock, right side closest to host rock, transect 1

Minerals

1. Hornblende (50%): Subhedral; coarse-grained (1-8mm)
2. Colorless amphibole (45%): Euhedral; fine-grained (0.5-6mm), larger grains exhibit acicular habit; zone of the fine-grained colorless amphibole share a boundary with zones of coarse-grained hornblende; undulatory extinction in some grains
3. Plagioclase (2%): Subhedral; medium grained (1-5mm); simple twinning present; undulatory extinction in some grains
4. Quartz (2%): Anhedral; undulatory extinction; fine-grained (1-3mm)
5. Titanite (1%): Euhedral; 1-3mm

Deformation Microstructures

- Relatively wavy thin section-wide fracture producing deformed, finer-grained mineral grains
- Transgranular fractures
- More intragrain fractures crosscutting length of hornblende grains than length of colorless amphibole grains
- Thin section-wide folding; more prominent in areas with more hornblende (there are distinct zones dominated with colorless amphiboles or hornblendes with distinct boundaries; the colorless amphibole-dominated zone does not contain hornblende clasts but the hornblende-dominated zone contains significant amounts of colorless amphibole grains)

Sample A16-04

Host amphibolite, left side closest to fault, transect 1

Minerals

1. Hornblende (80%): Subhedral; coarse-grained (2-10mm); simple twins in some grains; linearly oriented; epidotization of some grains
2. Plagioclase (10%): Subhedral to anhedral; fine- to medium-grained (0.5-2mm); contained in veins cross-cutting amphibole lineations; epidotization of some grains; simple and albite twinning present
3. Epidote (10%): Subhedral to anhedral; fine-grained (<0.5mm) where anhedral, medium-grained (1-4mm) where subhedral

Deformation Microstructures

- Veins present
- Transgranular fractures
- Significant intragrain fracturing in hornblende grains

Sample A16-05:

Host amphibolite, right side closest to fault, transect 1

Minerals

1. Colorless amphibole (60%): Euhedral to subhedral; fine-grained and wispy where subhedral (<0.5mm) to coarse-grained where subhedral (1-6mm); few fine grains seen in quartz vein; undulatory extinction in some grains
2. Hornblende (20%): Subhedral; coarse-grained (1-7mm); undulatory extinction in some grains
3. Quartz (10%): Anhedral; present as a vein; fine- to coarse-grained (0.5-10mm); subgrains present; evidence of grain boundary migration; undulatory extinction epidotization
4. Plagioclase (7%): Subhedral; medium-grained (1-5mm); simple and albite twins in some grains; epidotization
5. Epidote (3%): Anhedral; fine-grained (<0.5mm)
6. Chlorite (<1%): Anhedral; medium grained (1-3mm); apple green in PPL

Deformation Microstructures

- Veins present
- Thin section-wide folding
- Intragrain fractures in some quartz and plagioclase grains
- Few intragrain fractures crosscutting the length of hornblende grains

Sample A16-12

Host amphibolite, 64m away from the fault

Minerals

1. Hornblende (55%): Euhedral to subhedral; coarse-grained (1-10mm); linearly oriented
2. Epidote (45%): Subhedral; coarse grained (1-7mm); linearly oriented
3. Titanite (<1%): Euhedral; 1-2mm
4. Allanite (<1%): Euhedral to subhedral; 1-3mm
5. Unknown red oxide (<1%): Anhedral; 0.5-2mm

Deformation Microstructures

- Intragrain fractures crosscutting length of epidote grains; few in hornblende grains

Appendix III: Honor Code

I pledge on my honor that I have not given or received any unauthorized assistance or plagiarized on this assignment.

_____

Justine Giovanna Grabiec